JOURNAL OF GEOPHYSICAL RESEARCH, VOL. 101, NO. D2, PAGES 4299–4314, FEBRUARY 20, 1996

Long-term climate variability in a simple, nonlinear atmospheric model

M. V. Kurgansky, K. Dethloff, I. A. Pisnichenko, H. Gernandt,
F.-M. Chmielewski, and W. Jansen

Abstract. A nonlinear, baroclinic, hemispheric, low-order model of the atmosphere with nonzonal orographic and zonal thermal forcings has been constructed. The model is used to investigate the long-term climate variability by running it over 1100 years. The model runs show a chaotic behavior in a realistic parameter range. With and without a seasonal cycle in the thermal forcing, the model generates decadal climate variations which are of the same order as interannual variations. The maximum variability is found in a broad range of periods between 3 and 44 years. Empirical orthogonal function analysis reveals that these fluctuations are predominantly caused by the interaction between the orographically excited standing wave and the mean zonal flow. The computed power spectra of the principal component time series stress the importance of the high-frequency transients in long-term climate variability.

1. Introduction

While much has been learned in recent years about the factors that determine the behavior of the atmosphere, our understanding of its variability and long-term trends is still rather limited. The processes controlling climate are complex, and high-resolution paleorecords show pronounced variability on timescales of 10^4–10^6 years, as described by *Birchfield and Ghil* [1993] as well as on timescales of 10^1–10^3 years as discussed by *Mayewski et al.* [1993].

Whereas the variability on long timescales is connected with the slow, nonlinear physics of the ice sheets paced by the eccentric variability as pointed out by *Birchfield and Ghil* [1993] and *Berger et al.* [1993], the causes of the variability on the shorter timescales of 10^0–10^2 years are not yet understood. One of the essential problems in estimating man-made climatic change is to identify and understand the natural variability of the atmosphere on the aforementioned time scales and the reasons of these variabilities in terms of atmospheric physics.

The atmospheric circulation varies on a wide spectrum of timescales. The shorter synoptic variations dominate the fluctuations of the weather and originate in the internal dynamics of the atmospheric flow, which is unstable and strongly nonlinear. On timescales much larger than the synoptic there is a tendency to assume that variations are driven by external forcing, for example, solar cycle variations or coupling between the atmosphere and a more slowly varying component of the oceans. In investigations of climate sensitivity it is most important to determine the relative contributions of internal variability and external forcing. Much effort has been expended to study low-frequency variations on timescales of about a week to a month in the large-scale atmosphere [e.g., *Haines*, 1994]. This area has attracted intense research, since it spans a gap between short-term variations due to daily weather events and longer-term natural variations in the climate, whose mechanisms are mostly still the subject of speculation.

Can short-term variations of weather elements lead to significant long-term variability of the climate on timescales of 10^0–10^2 years? In order to answer this question we use an idealized atmospheric climate model, originally developed by *Tennekes* [1977] but never used for a systematic investigation of long-term climate variability.

The motivation for using simple, nonlinear climate models of the atmosphere is the expectation of understanding the long-term behavior of such a model more easily than that of a general circulation model, as was pointed out by *Ghil* [1988] and *Egger* [1992]. Simple models are computationally economical. Despite their low spatial resolution they show a complex temporal chaotic behavior in a realistic parameter range which resembles the dynamics of the atmosphere with frequent transitions between circulation states.

Similar investigations of the long-term variability by using a simple climate model have been carried out by *Pielke and Zeng* [1994] with the idealized nonlinear atmospheric model developed by *Lorenz* [1984, 1990]. *James and James* [1992] have discussed the problem with a multilevel baroclinic primitive equation model. We have constructed a simple baroclinic, low-order model which takes into account an orographically forced planetary wave and nonlinear interaction with a zonal flow excited by a meridional temperature gradient between the equator and the pole. We will show that such a simple model exhibits a behavior similar to the general circulation of the atmosphere and that it is suitable for studying features of long-term atmospheric variability. An attempt is made to discuss the importance of time variations on the scale of few weeks in the long atmospheric waves and the zonal flow due to nonlinear interactions between them leading to significant long-term climate changes.

The model formulation is based on a one-level, nondivergent model of the atmosphere with buoyant forcing which

[1]Institute of Atmospheric Physics, Russian Academy of Sciences, Moscow.
[2]Research Department, Alfred Wegener Institute for Polar and Marine Research, Potsdam, Germany.
[3]Meteorological Institute, Humboldt University, Berlin.
[4]Department of Nonlinear Dynamics, Potsdam University, Potsdam, Germany.

Paper number 95JD02703.
0148-0227/96/95JD-02703$05.00

imitates the baroclinic effects and with surface friction parameterization developed by *Tennekes* [1977]. *Alishayev* [1980, 1981] extended this model to divergent motions and considered the wind variations with altitude. The quasi-geostrophic version of this improved model is applied on a spherical Earth including orographic forcing, Newtonian cooling, and Ekman friction.

On the basis of this model we will discuss the natural variability of the model atmosphere due to the nonlinear internal dynamics using an integration over 400,000 days (1100 years). Experiments with and without an annual course of thermal forcing are compared in order to demonstrate the influence of seasonal changes in solar heating on the long-term variability.

The presented model is as complex as traditional two-level baroclinic models [e.g., *Galin and Kirichkov*, 1985]. In comparison with these it has the shortcomings of neglecting synoptic-scale baroclinic waves. The model and the results concerning stationary, periodic, and chaotic solution regimes are presented in sections 2 and 3. The structure of long-term climate variability is studied in section 4, using empirical orthogonal function (EOF) and principal component (PC) analysis. Conclusions are summarized in section 5.

2. Model Description

We consider a two-dimensional baroclinic atmosphere over the topography with height h governed by the equations of momentum, mass and energy conservation written here for simplicity in Cartesian (x, y) coordinates, similar to *Alishayev* [1980]:

$$\frac{D}{Dt}u = -\frac{R}{\rho}\frac{\partial}{\partial x}(\rho T) - g\frac{\partial}{\partial x}h + fv + F_x, \tag{1}$$

$$\frac{D}{Dt}v = -\frac{R}{\rho}\frac{\partial}{\partial y}(\rho T) - g\frac{\partial}{\partial y}h - fu + F_y, \tag{2}$$

$$\frac{D}{Dt}\rho = -\rho\left(\frac{\partial}{\partial x}u + \frac{\partial}{\partial y}v\right), \tag{3}$$

$$\frac{D}{Dt}T = -\gamma T\left(\frac{\partial}{\partial x}u + \frac{\partial}{\partial y}v\right) + I. \tag{4}$$

Here $\rho = P/g$, where P is the surface air pressure and g is the gravitational acceleration; $\gamma = R/c_p = 2/7$, where R is the gas constant of dry air and c_p is the specific heat capacity at constant pressure; T is the average temperature of individual air columns; F_x and F_y are the longitudinal (x) and latitudinal (y) components of mechanical forcing, including friction; I is the thermal forcing; f is the Coriolis parameter; u and v are the x and y components of velocity; and

$$\frac{D}{Dt} = \frac{\partial}{\partial t} + u\frac{\partial}{\partial x} + v\frac{\partial}{\partial y}$$

is the operator of the total derivative with respect to time.

These equations are obtained by averaging the three-dimensional hydrothermodynamical, quasi-static equations with respect to height, assuming that the horizontal wind field and potential temperature field do not significantly change in the vertical direction. This rough approximation disregards the coupling between horizontal and vertical components of motion resulting from the thermal wind relation. So strictly speaking, equations (1)–(4) are to be considered as a correction to barotropic equations, taking into account small effects of horizontal inhomogeneity in the temperature field. Nevertheless, they give surprisingly good results, as was already mentioned by *Tennekes* [1977], who gives a physical interpretation of the zonal flow instability mechanism resulting in this model. The mean western zonal wind is maintained by thermal forcing. Relatively warm (and light) air masses are deviated poleward by the Coriolis force, and relatively cold (and heavy) air masses are deviated equatorward. This is the case of so-called horizontal large-scale convection in the Coriolis force field.

Using the quasi-geostrophic approximation and eliminating the horizontal wind divergence, (1)–(4) become

$$\frac{\partial}{\partial t}(\nabla^2\psi - L^{-2}\psi) + J(\psi, \nabla^2\psi + f + ghf_0^{-1}L^{-2}) = -L^{-2}\frac{\partial}{\partial t}\tau + J(\tau, ghf_0^{-1}L^{-2}) + \frac{\partial}{\partial x}F_y - \frac{\partial}{\partial y}F_x, \tag{5}$$

$$\frac{\partial}{\partial t}\tau + J(\psi, \tau) = \varepsilon\frac{\partial}{\partial t}\psi - \varepsilon J(\psi, ghf_0^{-1}) + Rf_0^{-1}(1+\gamma)^{-1}I, \tag{6}$$

where $L^2 = R\bar{T}f_0^{-2}$ is the baroclinic Rossby radius, $\varepsilon = \gamma/(1+\gamma) = 2/9$, and J and ∇^2 denote the Jacobian and the Laplacian operator, respectively. Furthermore,

$$\psi = R\bar{T}f_0^{-1}\{(P-\bar{P})/\bar{P} + (T-\bar{T})/\bar{T}\} + ghf_0^{-1}$$

is the stream function, and

$$\tau = R(T-\bar{T})f_0^{-1}$$

is proportional to the deviation of the temperature T from the average air temperature $\bar{T} = 250$ K of the entire atmosphere; $f_0 = 10^{-4}$ s^{-1} is the Coriolis parameter reference value and $\bar{P} = 1012.5$ hPa is the average surface air pressure. Equations (5)–(6) are comparable in complexity with traditional two-layer models, but more accurately describe planetary-scale, low-frequency processes.

If (5)–(6) are integrated over the entire atmosphere, the energy balance equation will readily be obtained:

$$\frac{d}{dt}E = \int\int\left\{-\psi\left(\frac{\partial}{\partial x}F_y - \frac{\partial}{\partial y}F_x\right) + c_pI(T-\bar{T})/\bar{T}\right\}dx\,dy.$$

Here,

$$E = \frac{1}{2}\int\int\left\{(\nabla\psi)^2 + c_p\bar{T}((T-\bar{T})/\bar{T})^2 + R\bar{T}\left(\frac{P-\bar{P}}{\bar{P}} + \frac{gh}{R\bar{T}}\right)^2\right\}dx\,dy$$

is the sum of kinetic energy and a specific form of the available enthalpy [see, e.g. *Dutton*, 1973; *Pearce*, 1978; *Kurgansky*, 1981; *Marquet*, 1991].

In the limit $L^{-2} \Rightarrow 0$, equation (5) is reduced to the non-divergent vorticity equation

$$\frac{\partial}{\partial t}\nabla^2\psi + J(\psi, \nabla^2\psi + f) = \frac{\partial}{\partial x}F_y - \frac{\partial}{\partial y}F_x. \tag{7}$$

In this way the effects of horizontal baroclinity (buoyancy), large-scale compressibility, and orographic impact appear in the same order as L^{-2}. Equation (7) can also be derived directly using the three-dimensional equations of a barotropic

atmosphere (with the constant values of potential temperature over all the atmosphere) under the following two assumptions: (1) Earth's surface corresponds to an approximately isobaric level, i.e. disregarding the effect of the mean wind divergence, and (2) weak altitude dependence of the wind field. A more realistic model is the so-called equivalent-barotropic model [*Charney*, 1949], where horizontal wind can change its magnitude with altitude, but not the direction:

$$u(x, y, p, t) = A(p)u_0(x, y, t),$$

$$v(x, y, p, t) = A(p)v_0(x, y, t),$$

where $A(p)$ is some prescribed function of pressure p.

In this case, instead of equation (7), the result is

$$\frac{\partial}{\partial t}\nabla^2\psi + J(\psi, k\nabla^2\psi + f) = \frac{\partial}{\partial x}F_y - \frac{\partial}{\partial y}F_x. \tag{8}$$

Here,

$$k = P\int_0^P A^2\,dp \Big/ \left(\int_0^P A\,dp\right)^2 > 1$$

according to Cauchy-Schwartz's inequality. If, for example $A = (P - p)/P$, then $k = 4/3$. In analogy to (8) we introduce the parameter k into (5). The direct procedure of introducing such a parameter into (1)–(4) and (5)–(6) would be more complicated. However, using the quasi-geostrophic scaling arguments, it can be shown that the expression obtained for k is valid in the general case. We have taken $k = 4/3$ and adopted the parameterizations for external factors of Newtonian cooling and Ekman friction as follows:

$$RIf_0^{-1}(1 + \gamma)^{-1} = \chi(\tau^* - \tau),$$

$$\frac{\partial}{\partial x}F_y - \frac{\partial}{\partial y}F_x = -\nu_E\nabla^2(\psi - \tau).$$

Here χ is the coefficient of Newtonian cooling, τ^* is the reference radiative equilibrium temperature, and ν_E is the coefficient of Ekman friction. Using $k > 1$, the threshold for the long-wave baroclinic instability is reduced compared with the case $k = 1$. More important, it gives the shortwave instability cutoff.

Considering the mentioned above parameterizations the equations (5)–(6) can be written in a spherical geometry and in a nondimensional form by using the Earth's radius a as a unit of length and the inverse of Earth's rotation angular velocity Ω as a unit of time:

$$\frac{\partial}{\partial t}(\nabla^2\psi - \Lambda^2\psi) + J(\psi, k\nabla^2\psi + 2\mu + \Lambda^2\mathrm{H}) = -\Lambda^2\frac{\partial}{\partial t}\tau + \Lambda^2 J(\tau, \mathrm{H}) + C\nabla^2(\tau - \psi), \tag{9}$$

$$\frac{\partial}{\partial t}\tau + J(\psi, \tau) = \varepsilon\frac{\partial}{\partial t}\psi - \varepsilon J(\psi, \mathrm{H}) + Q(\tau^* - \tau). \tag{10}$$

Here μ is the sine of geographic latitude. The nondimensional radius of deformation Λ^{-1} is determined by $\Lambda^2 = a^2L^{-2}$ ($\Lambda^2 = 5.656$); the nondimensional Ekman and Newtonian damping coefficients are $C = \nu_E/\Omega$ and $Q = \chi/\Omega$, respectively. $\mathrm{H} = (1/\sqrt{2})gha^{-2}\Omega^{-2}$, and $f_0 = \Omega\sqrt{2}$.

Equations (9)–(10) are further rewritten for a convenient time integration as follows:

$$\frac{\partial}{\partial t}(\nabla^2\psi - \Lambda^2(1 - \varepsilon)\psi) + J(\psi, k\nabla^2\psi + 2\mu + \Lambda^2\mathrm{H}(1 - \varepsilon) - \Lambda^2\tau) - J(\tau, \Lambda^2\mathrm{H}) - C\nabla^2(\tau - \psi) + \Lambda^2 Q(\tau^* - \tau) = 0, \tag{11}$$

$$\frac{\partial}{\partial t}(\nabla^2\tau - \Lambda^2(1 - \varepsilon)\tau) + (\nabla^2 - \Lambda^2)J(\psi, \tau) + \varepsilon J(\psi, k\nabla^2\psi + 2\mu) + \varepsilon\nabla^2 J(\psi, \mathrm{H}) - \varepsilon\Lambda^2 J(\tau, \mathrm{H}) - \varepsilon C\nabla^2(\tau - \psi) - Q(\nabla^2 - \Lambda^2)(\tau^* - \tau) = 0. \tag{12}$$

The dependent variables are expanded into spherical harmonics:

$$\psi(\lambda, \mu, t) = -\alpha(t)\mu + F(t)P_N^0(\mu) + A(t)P_n^m \sin m\lambda + K(t)P_n^m \cos m\lambda$$

$$\tau(\lambda, \mu, t) = -\beta(t)\mu + G(t)P_N^0(\mu) + B(t)P_n^m \cos m\lambda + L(t)P_n^m \sin m\lambda$$

where λ is the longitude and $P_n^m(\mu)$ are the normalized associated Legendre polynomials ($P_1^0 = \sqrt{(3/2)}\mu$). The zonal wave number (order) is m, and n (N) corresponds to the total wave number (degree). The values N, $n - m$ are odd integers that make the model hemispheric. We are using a low-order model with a very sparse horizontal resolution of wave number m in the zonal direction. Here $n - m$ characterizes the number of zeroes in the stream function field from pole to pole. The orography and thermal forcing are as follows:

$$\mathrm{H} = \mathrm{H}_0P_n^m(\mu)\sin m\lambda, \qquad \tau^* = -\beta^*\mu.$$

Equations (11)–(12) in their spectral form are shown in Appendix A. Here we note only that the spectral version of the model consists of eight ordinary. quadratically nonlinear differential equations.

Equation (A6) includes an additional thermal forcing due to surface baroclinity. It is twice as large as orographic forcing, acts in the opposite direction, and corresponds to radiative cooling over topographic maxima and warming over minima, respectively. In all of the later runs described we adopt $m = 2$, $n = 5$, and $N = 3$.

The seasonal course in external thermal forcing can be taken into account by

$$\beta^* = \beta_0^*(1 + \mathrm{E}\sin(t/365)). \tag{13}$$

E describes the modulation of the meridional temperature gradient. The resulting nonautonomous system of eight equations is transformed to the autonomous system of 9 equations by introducing the additional variable $\Theta(t)$:

$$\beta^* = \beta_0^*(1 + \mathrm{E}\sin(\Theta/365))$$

It applies to $(d/dt)\Theta = 1$ and $\Theta = 0$ for $t = 0$.

3. Initial Experiments

Model equations have been integrated by means of a fourth-order Runge-Kutta algorithm with time steps of 1 hour. Initial conditions were chosen such that without nonlinear terms and in the absence of orography the solution would be in balance with the external forcing. The wave components were excited

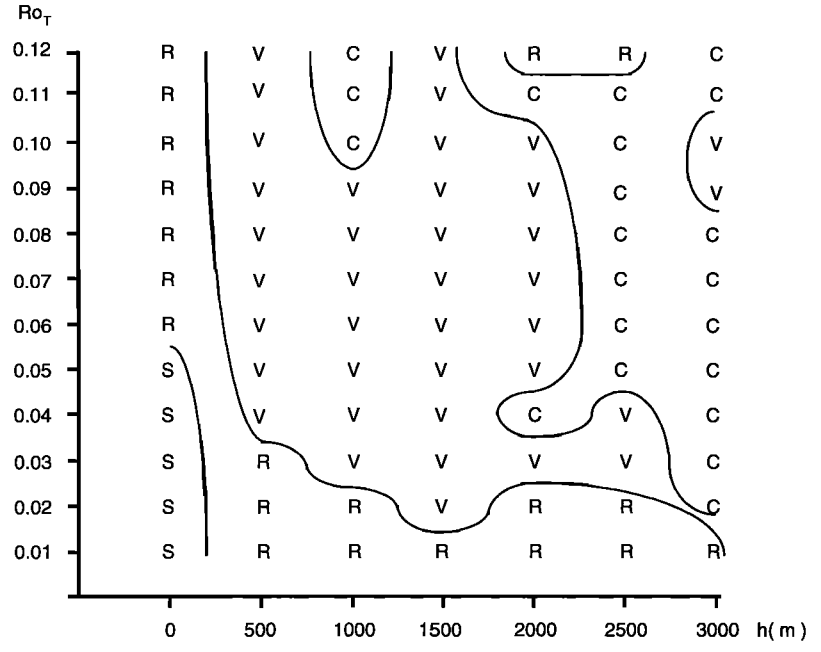

Figure 1. Bifurcation diagram as function of the meridional temperature gradient between equator and pole, described by the thermal Rossby number Ro_T and the orographic height h (meters) for $m = 2$, $n = 5$, $N = 3$ and dissipation time of 16 days. Symbols are S, stationary solutions; R, Rossby-wave-like solutions with constant amplitudes; V, periodic vacillation regime; and C, chaos.

to give a meridional heat flux for the starting time. In order to solve the initial problem in the conservative case, the exact solution of the nonlinear problem in terms of elliptic functions was studied for $k = 1$, $\alpha = \beta = \text{const}$, $n = N = 5$, $H_0 = 0$ and applied to test the numerical procedure (see Appendix B).

We integrated the model equations over 1000 days and visually separated the solution regimes into stationary (S), Rossby-wave-like solutions with constant amplitudes (R), periodic vacillations (V), and chaotic regimes (C). We also specified the influence of the damping scale, which was recognized to be of minor importance. The model runs were performed with $\nu_E = \chi$ taking a dissipation timescale of 16 days.

As a first result we have constructed bifurcation diagrams as a function of the temperature gradient between equator and pole and the orographic height h. The temperature gradient is used in a nondimensional form by the so-called thermal Rossby number $Ro_T = R\Delta T f_0^{-1}\Omega^{-1}a^{-2}$, where ΔT is the temperature difference between the equator and the pole. $Ro_T \cong 0.001\ \Delta T$ if ΔT is in degrees Celsius.

The results are presented for wave numbers $m = 2$, $n = 5$, and $N = 3$ in Figure 1. The diagram shows islands of chaotic behavior for realistic values of the meridional temperature gradient and orographic height. If the dissipation is doubled there is no structural change in the resulting bifurcation diagram.

Examples of temporal behavior of the nondimensional amplitude $\alpha(t)$ of the mean angular velocity of the atmosphere are shown for a constant orographic height of 2500 m and temperature differences between equator and pole of 20°C, 25°C and 70°C in Figures 2, 3, and 4. They describe the Rossby wave regime, the vacillation regime, and the chaotic regime.

The solutions in the chaotic regime are now investigated in more detail. In order to be sure that the model is really in a chaotic regime, we have specified the parameter values for meridional temperature gradients and orographic heights from diagrams like Figures 2, 3, 4. Using a temperature difference of 70°C between equator and pole and an orographic height of 2500 m we integrated the model over 400,000 days, on about 1100 years, and called it run 1.

In Figure 5 we show the climate of the model, computed by averaging the stream function field over the model integration time of 1100 years excluding the first 10 years. At midlatitudes, well-developed lows and less pronounced highs are seen. The highs are situated near the maximum heights of the orography.

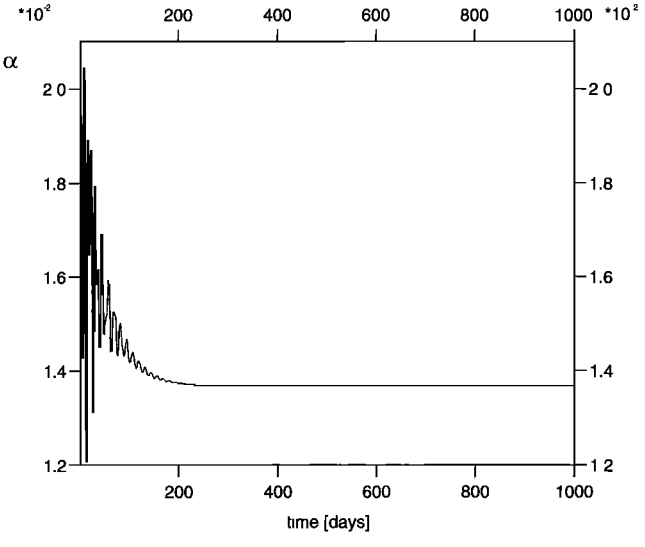

Figure 2. Temporal evolution of $\alpha(t)$ in the Rossby regime (R) for $m = 2$, $n = 5$, $N = 3$, $h = 2500$ m, and $Ro_T = 0.02$ (20°C).

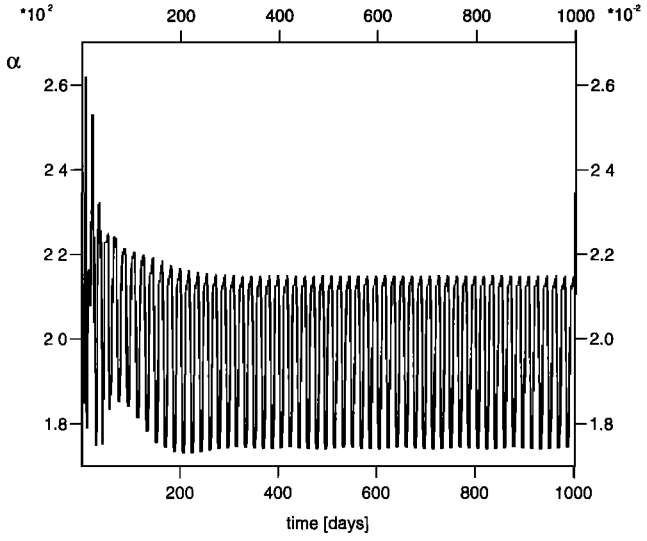

Figure 3. Temporal evolution of $\alpha(t)$ in the vacillation regime (V) for $m = 2$, $n = 5$, $N = 3$, $h = 2500$ m, and $Ro_T = 0.025$ (25°C).

In midlatitudes the general features of model climatology agree with the climatological mean stationary waves described by *Wallace* [1983] using observational data.

To characterize the chaotic regime in a quantitative manner, we computed the Lyapunov exponents using a modification of the method by *Shimada and Nagashima* [1979]. One of the eight Lyapunov exponents is positive, one is zero, and six are negative. The value of the positive exponent corresponds to an e-folding time of about 7.6 days. The sum of all exponents is negative and corresponds to an e-folding time of about 2.5 days. In Figure 6 the positive time dependent Lyapunov exponent is plotted against the logarithm of the time integration period. The plot shows how the time dependent exponent converges to the Lyapunov exponent of the model. The dimension of the attractor resulting in the model has been determined following *Kaplan and Yorke* [1979]. A Kaplan-Yorke

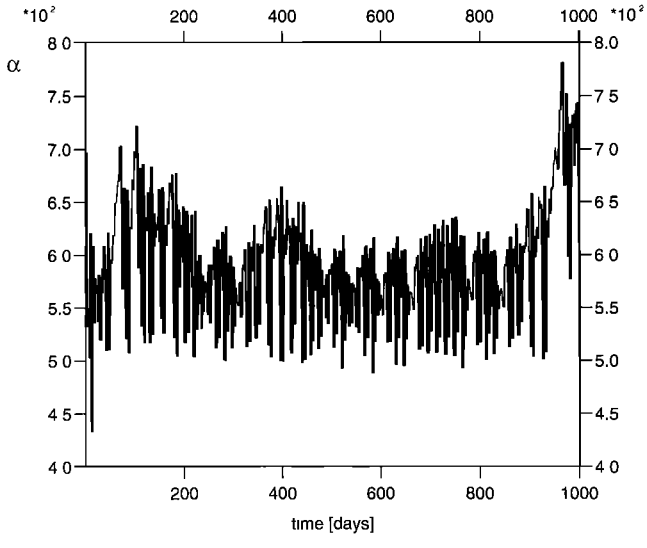

Figure 4. Temporal evolution of $\alpha(t)$ in the chaotic regime (C) for $m = 2$, $n = 5$, $N = 3$, $h = 2500$ m, and $Ro_T = 0.07$ (70°C), for the first 1000 days of integration.

dimension of 5.3 was found. This value may be considered as an indication of the Hausdorff dimension of the attractor. It suggests that the described chaotic behavior would have been simulated by a dynamical system with only 6 degrees of freedom.

Figure 7 shows the temporal changes in the zonal index $\alpha(t)$ over the first 10,000 days of run 1. Transitions between different circulation states of varying duration are visible.

Daily data series of $\alpha(t)$ over 400,000 days have been used to compute the power spectrum P_α of the zonal index. The result is shown in Figure 8 together with the half width of the 95% confidence interval. The standard deviation σ of the time mean $\bar{\alpha} = 0.062$ is equal to 0.0062. A strong perturbation ranging 30% in the initial conditions did not change the spectrum in Figure 8 significantly. There are two separated frequency maxima with periods of approximately 8 days and 25 days. The plot shows that the amplitude of the fluctuations steadily increases as the period increases from the seasonal timescale to interannual timescales. The most pronounced signals are seen for periods of approximately 3, 6, 13–14, 23, and 44 years. The maximum variability was found in the decadal timescale. The robustness of the different frequency peaks has been examined by using different fast Fourier transform (FFT) resolution 2^N in Matlab. All results described have been determined at a resolution with $N = 16$. Spectrum estimations with different N lead to small changes in the position of the frequency peaks.

4. Structure of the Long-Term Climate Variability

In the previous section we discussed the long-term chaotic variability of the model on the basis of power spectrum and Lyapunov exponents computations. Now we apply an empirical orthogonal function (EOF) analysis to determine the most significant structures in the fluctuations of the stream function fields. A set of EOFs for a time series is generated by determining the eigenvalues and eigenfunctions of the covariance matrix which is defined by the stream function values on a grid with a spacing 18° latitude by 45° longitude. In our low-order model, only four independent stream function field components have been considered. Therefore only the first four eigenvalues are nonzero, which explain 99.99% of variance. The time series can be represented compactly by projecting the stream function field at any time level on the set of EOFs. The time series of amplitudes of the ith EOF are called the ith principal component (PCi) of the time series.

In the following we discuss the EOF patterns and the power spectra of the corresponding PCs for Run 1. EOF 1 explains 65.0% of the total variance of the stream function fields, EOF 2 explains 32.4%, EOF 3 explains 2.3%, and EOF 4 explains 0.3%. The structure of EOFs 1, 2, 3, and 4 is shown in Figure 9. EOFs 1 and 2 describe regimes with well-pronounced wave structures. EOF 1 is in phase with the orography. In comparison to EOF 1, EOF 2 is shifted by 45° in longitude. EOFs 3 and 4 describe the zonal regimes.

The corresponding power spectra of PC 1, PC 2, PC 3, and PC 4 are shown in Figure 10. They specify the timescales of the EOF's variability. PC 1 (Figure 10a) shows well-pronounced maxima at time periods of 16 and approximately 25 days. Because the pattern of EOF 1 coincides with the contours of orography, these synoptic variations seem to be controlled by the orographic instability. In addition to these timescales there is a broad spectrum of frequency peaks in the interannual scale

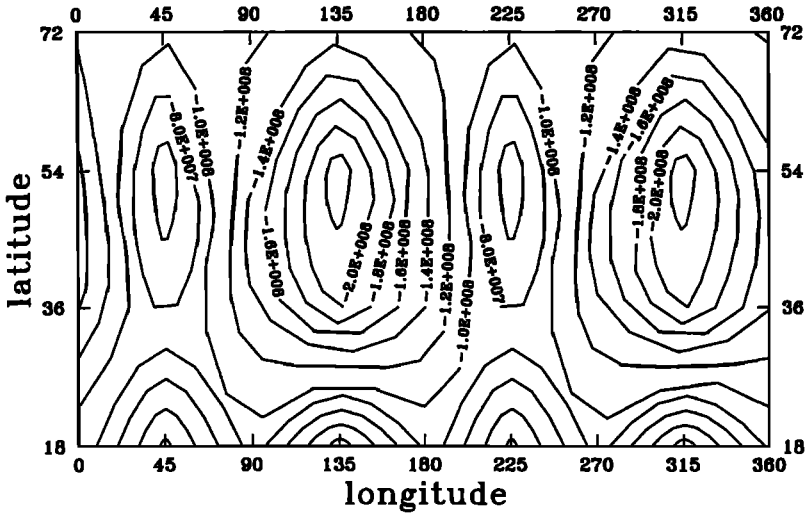

Figure 5. Run 1: Climatology of the stream function ψ (m^2/s) for $m = 2$, $n = 5$, $N = 3$, $h = 2500$ m, and $Ro_T = 0.07$ (70°C) without a seasonal cycle.

between 3 and 44 years. Although *James and James* [1992] investigated the time variability in the zonally averaged winds, the ultralow-frequency variability associated with the large-scale structure described by EOF 1 looks very similar to those obtained by these authors.

In contrast, PC 2 does not show any long-term variability. Its frequency peaks are confined to synoptic scales between 10 and 30 days. A coupling exists between PC 1 and PC 2 in these timescales due to the orographic instability. Both PC 3 and PC 4 show ultralow-frequency variability similar to that of PC 1, connected with amplitude changes in the standing components of the large-scale circulation patterns. They are presented in Figures 10a, 10c, and 10d. In PC 3, frequency peaks occur in the synoptic timescales with maximum amplitudes at 8 days which are connected with the baroclinic instability of the zonally mean state present in EOF 3.

Both EOF 1 and EOF 3 are responsible for the major part of ultralow-frequency variability. The EOFs show that this climate variability is caused by the interaction between the mean zonal flow, described by EOF 3 and the wave component EOF 1. EOF 2 is shifted by 45° longitude relative to EOF 1 and is involved only in the variability on synoptic timescales with periods smaller as 1 month.

We will turn now to run 2 with the inclusion of a seasonal cycle. This was achieved by varying the equator-pole temperature difference sinusoidally in time with a period of 365 days and an amplitude of 20 K. It corresponds to $E = 2/7$ in the equation (13) and describes a radiative temperature difference

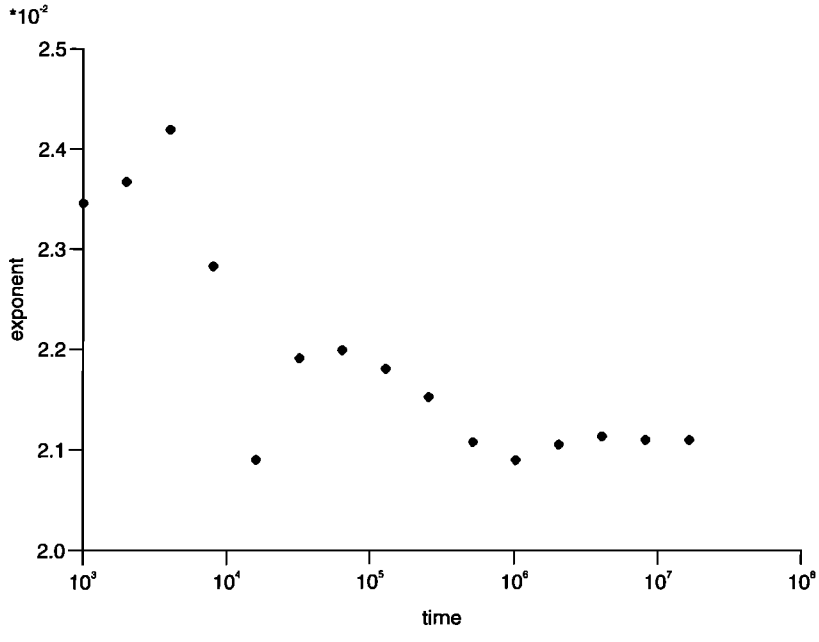

Figure 6. Convergence of the positive Lyapunov exponent. The time is given in nondimensional units. Number of days is time/2π.

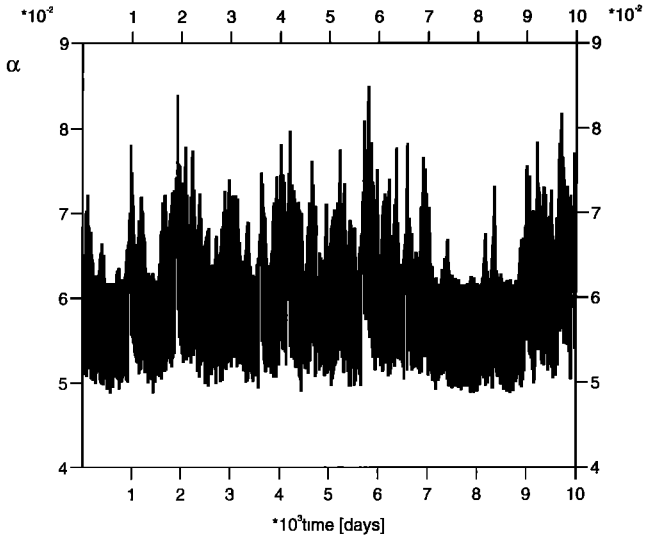

Figure 7. Temporal evolution for the first 10,000 days of integration of the zonal index $\alpha(t)$ in the chaotic regime for $m = 2$, $n = 5$, $N = 3$, $h = 2500$ m, and $Ro_T = 0.07$ (70°C).

of 40 K between winter and summer following *James and James* [1992]. All other parameters are the same as for run 1.

The averaged stream function for the model run 2 over 1100 years is shown in Figure 11. Figure 12 shows the corresponding power spectrum P_α computed on the basis of daily data series of the zonal index $\alpha(t)$. The seasonal cycle has been removed. As in Figure 8 there are two separated frequency maxima for periods of approximately 8 days and 25 days. In run 2 the model again shows a large variability on a decadal timescale. The most pronounced peaks occur near 3, 13, and 26 years. The seasonal cycle changed the individual frequency peaks in comparison with run 1, but the ultralow-frequency variability in the decadal timescale remains.

The EOFs were computed using stream function fields without removing the seasonal cycle. This has the advantage for the case of PCs being considered as the variables of a dynamical system constructed on the basis of EOFs. Time series of PCs were computed, the seasonal cycle was excluded, and the power spectra were calculated.

EOF 1 explains 59.9% of the total variance of the stream function fields, and EOFs 2, 3, and 4 explain 32.6%, 6.3%, and 1.2%. The structure of EOFs 1, 2, 3, and 4 is shown in Figure 13 and is quite similar to that of the EOF's from run 1 without the seasonal cycle. EOFs 1 and 2 again describe regimes with well-pronounced wave structures. EOF 4 describes a zonal regime. In comparison with run 1, the only difference occurs in EOF 3, which does not describe a zonal regime but a circulation state with a wave structure.

The power spectra of PC 1, PC 2, PC 3, and PC 4 are presented in Figure 14. They show that the ultralow-frequency variability is described by PC 1 and PC 3. The mean seasonal cycle in PCs, not presented here, is much less pronounced in PC 2 than in PC 1 and in PC 3. However, an anticorrelation in seasonal cycles of PC 1 and PC 2 is still seen. It shows that the seasonal forcing influences the synoptic variability of the model.

The intercomparison of both EOF analysis for run 1 and run 2 leads to the suggestion that the attractor of the system remains structurally unchanged. A deformation does occur, which appears in the structures of EOF 3 and the power spectra. Its magnitude is proportional to the amplitude of the seasonal cycle of the equator to pole temperature difference. The additional run 3 with a smaller temperature amplitude of 10 K for the seasonal forcing confirms this suggestion.

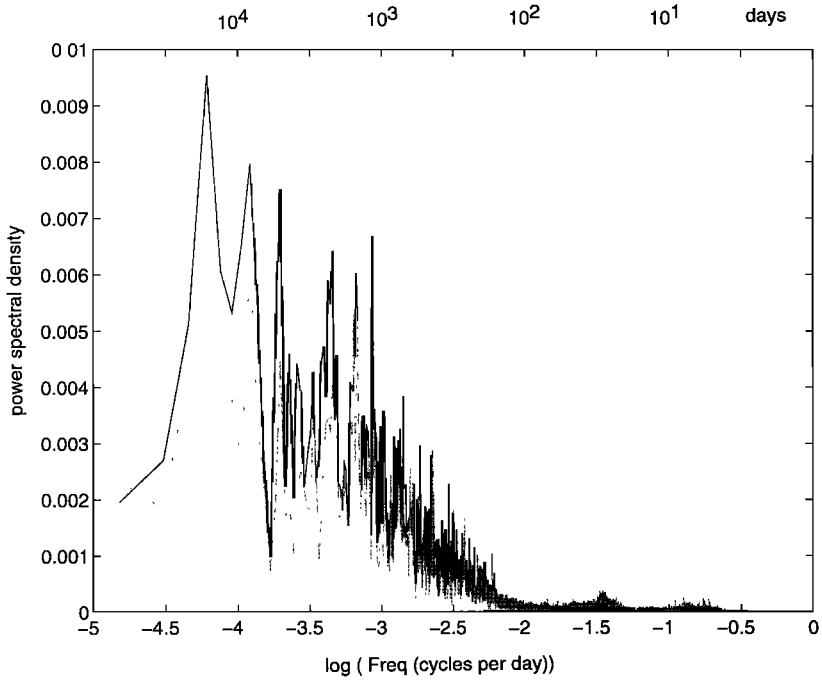

Figure 8. Run 1: Power spectrum P_α as a function of the logarithm of frequency computed from 400,000 days of α for $m = 2$, $n = 5$, $N = 3$, $h = 2500$ m, and $Ro_T = 0.07$ (70°C) without seasonal forcing. The power spectrum is shown by the bold black line, and the half width of the 95% confidence interval is shown by the thin gray line.

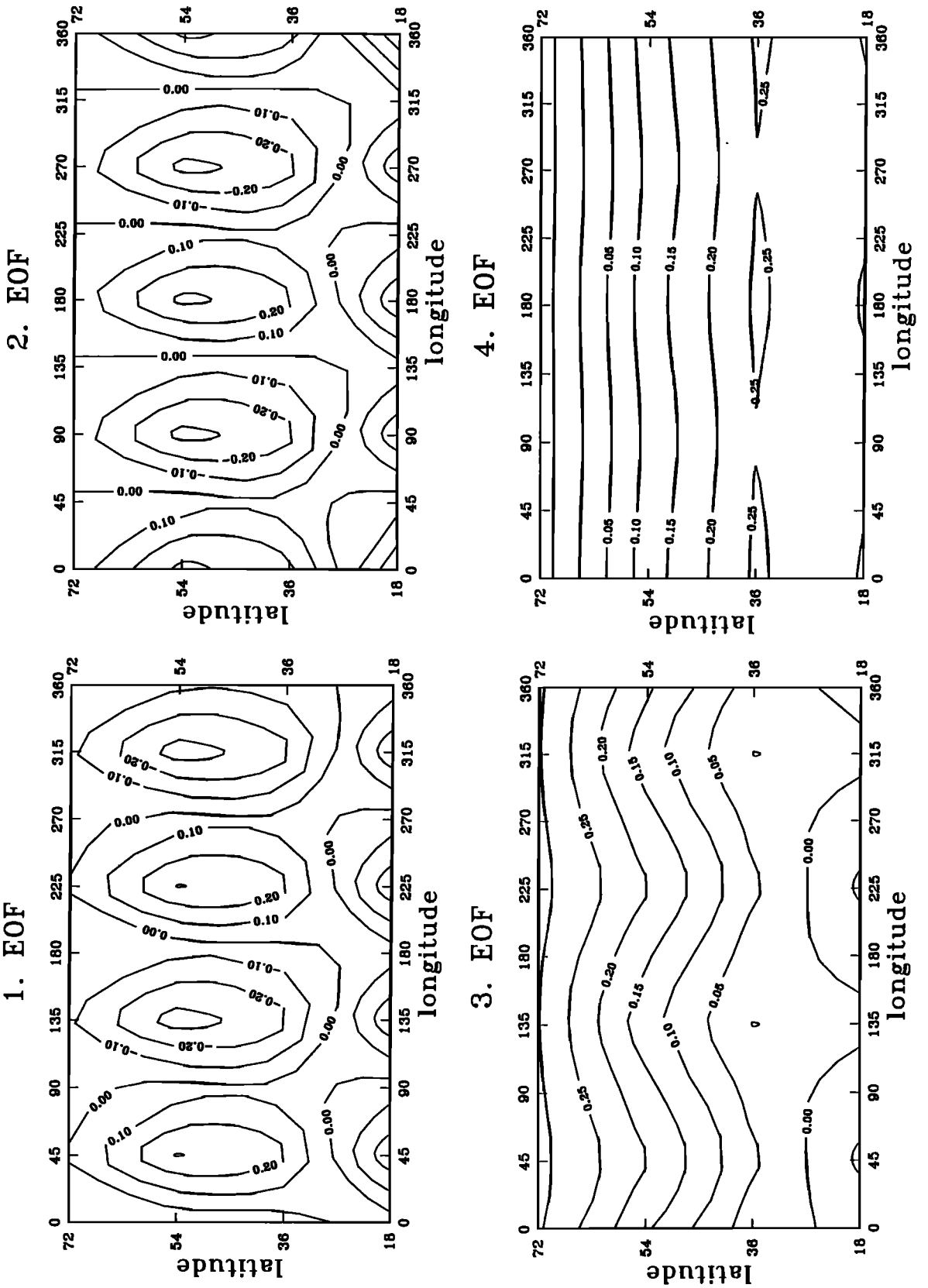

Figure 9. Run 1: Structure of EOFs 1, 2, 3, and 4. The EOFs are normalized by unity.

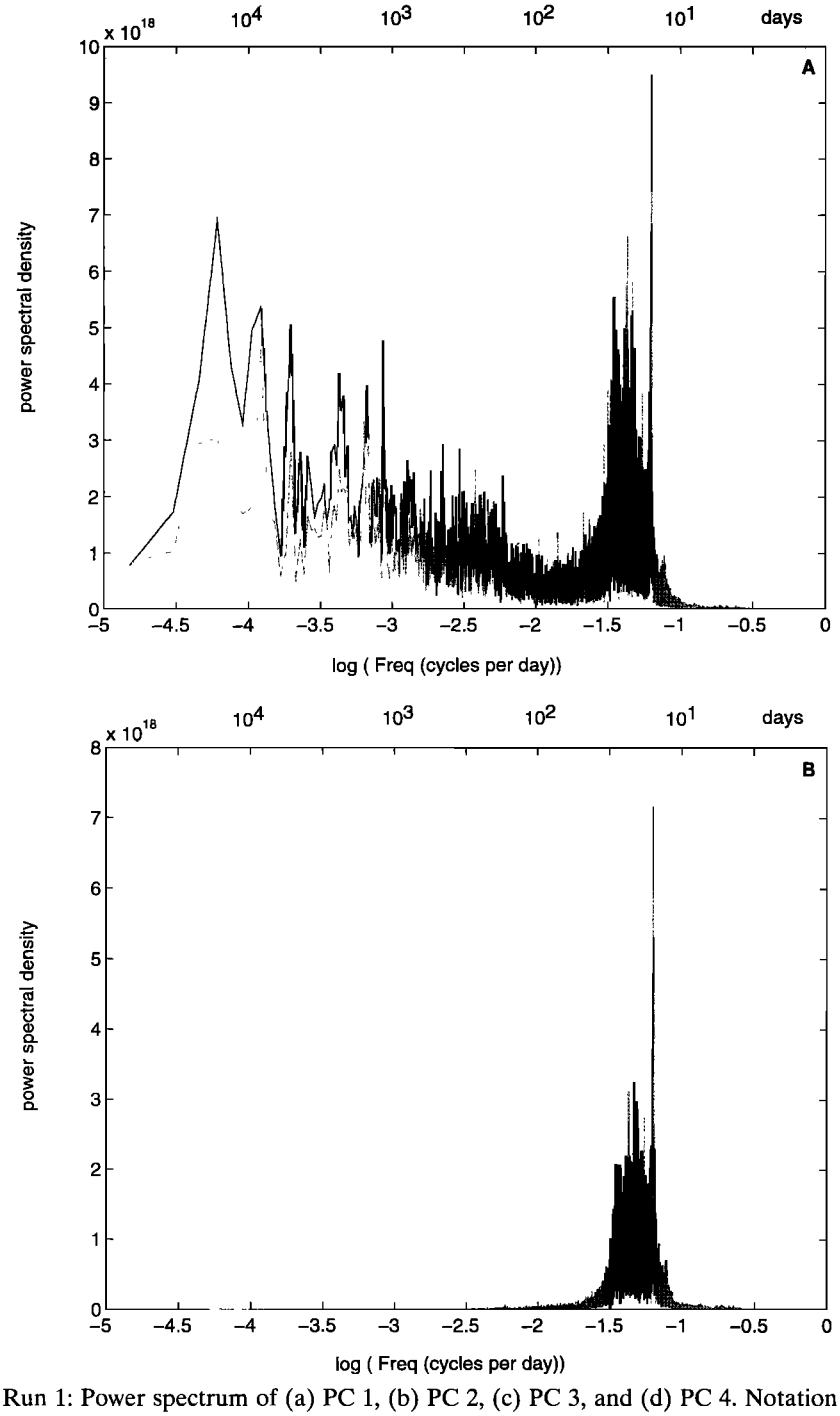

Figure 10. Run 1: Power spectrum of (a) PC 1, (b) PC 2, (c) PC 3, and (d) PC 4. Notation as in Figure 8.

For run 1 we calculated the total variance σ_α^2 of daily time series of α and also the portions of σ_α^2 in percents, which fall into four intervals of periods: 2 to 6 days, 6 days to 1.1 year, 1.1 year to 11 years; and 11 years to 1100 years. Results are summarized in Table 1. On the basis of the PC 1 and PC 2 power spectra, which are quite similar in their high-frequency part, we are able to give a rough estimate of the percentage of the σ_α^2 that falls at periods of less than 1 year. It is twice as large as the percentage of EOF 2 and is equal to approximately 65%. The sum of percentages from the first two rows in Table 1 gives a very close estimate of 66%. In the case of seasonal forcing the total variance σ_α^2 has been increased 3.91 times. Its distribution on the aforementioned intervals of periods is shown in the second column of Table 1.

5. Conclusions

We constructed a simple baroclinic hemispheric low-order model of the atmosphere on the basis of quasi-geostrophic equations. They include orographic forcing in the long wave and thermal forcing in the zonal components. The model consists of eight components and uses the spherical harmonics Y_1^0, Y_3^0, $Y_5^{\pm 2}$. We estimated the bifurcation properties of the model as a function of orographic height h and meridional tempera-

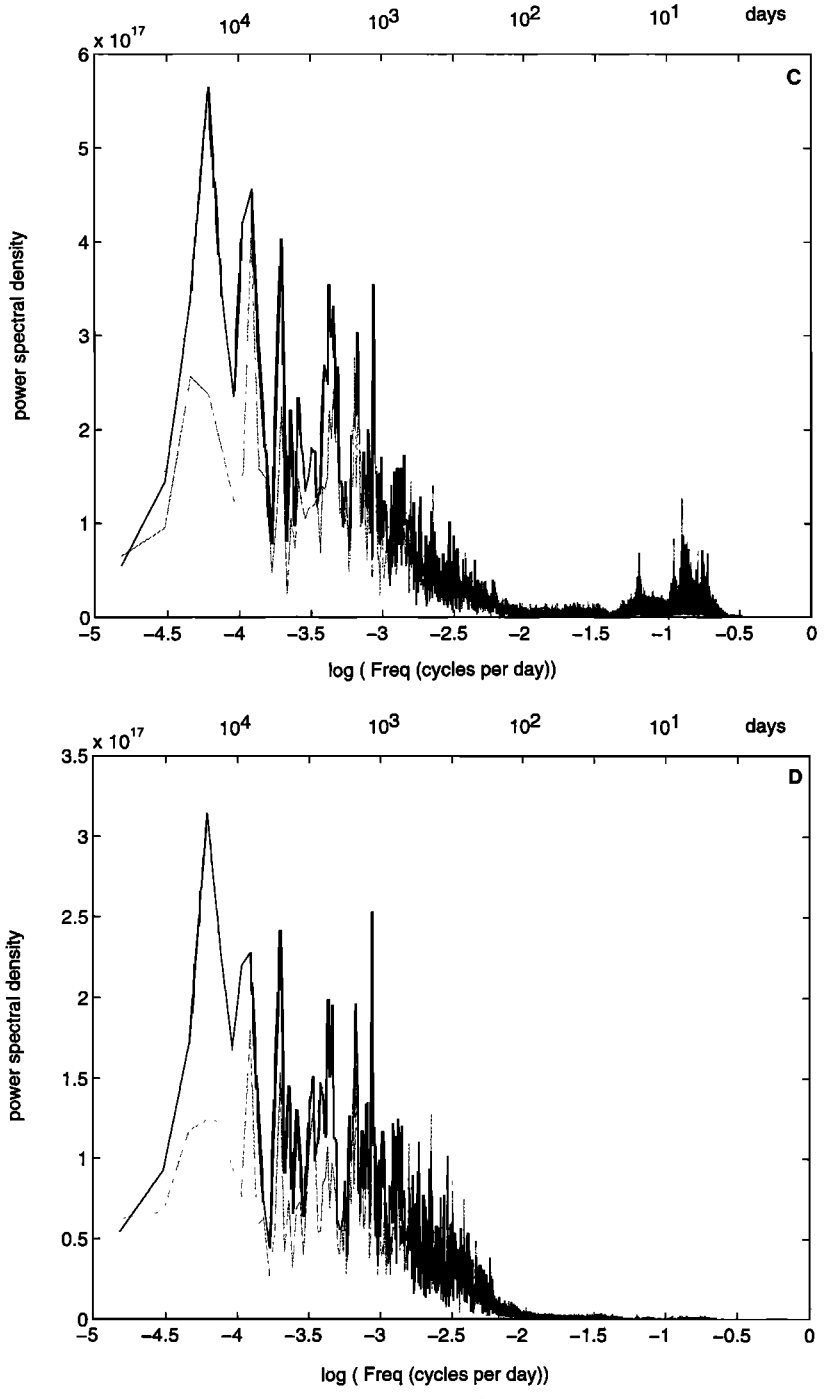

Figure 10. (continued)

ture difference between equator and pole ΔT. For realistic parameter values of $h = 2500$ m and $\Delta T = 70°C$ we found chaotic behavior.

To determine this in a quantitative manner we computed the Lyapunov exponents. One Lyapunov exponent is positive, which indicates the chaotic behavior of the model. The Kaplan-Yorke dimension of the attractor has been determined as 5.3. This value is comparable to the estimated attractor dimension of 6 or 7 in a simplified general circulation model described by *James and James* [1992]. In this sense we constructed a low-order model with the minimum of degrees of freedom needed for producing long-term climate variability. The temporal behavior of the model resembles the dynamics of the atmosphere with frequent transitions between different circulation states.

Then the model was integrated with and without a seasonal cycle over 1100 years in the chaotic regime. The climate of the model by averaging over the entire time period was determined. Power spectra computations of the zonal index showed frequency peaks between 3 and 44 years without seasonal cycle and between 3 and 26 years with included seasonal cycle. This ultralow-frequency variability in the decadal time is produced by the nonlinear atmospheric dynamics only.

Empirical orthogonal function analysis of the stream func-

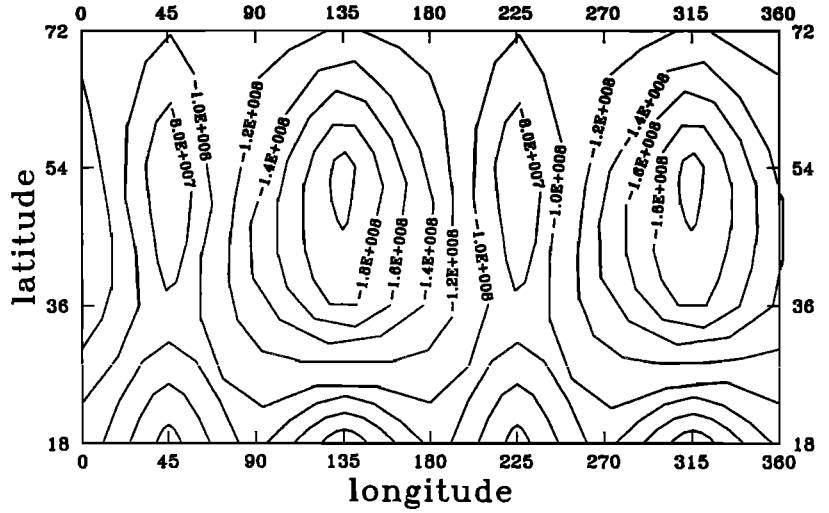

Figure 11. Run 2: Climatology of the stream function ψ (m^2/s) for $m = 2$, $n = 5$, $N = 3$, $h = 2500$ m, and $Ro_T = 0.07$ (70°C) with a seasonal cycle.

tion fields together with the power spectra calculations of the principal components showed that the nonlinear interactions between EOFs 1, 3, and 4 determine the ultralow-frequency variability in the decadal timescale. The interactions between EOFs 1, 2, and 3 determine the low-frequency variability on timescales from 10 days up to a month.

Well-pronounced maxima in the power spectra of the principal components occur at 16 and 25 days. Similar periods have been noted in observational data. This gives confidence in the conclusions concerning the ultralow-frequency variability of the model.

Branstator and Held [1995] explained the 25-day pattern as a barotropically unstable wave dominated in most winters by Y_4^1 and sometimes by Y_5^2. The latter wave has been used in our current model. In future investigations it would be interesting to run the model with the basic wave Y_4^1 used by *Branstator and Held* [1995].

The estimated temporal structure of ultra-low frequency variability in our model resembles in many features that of *James and James* [1992] in the decadal timescale.

Lorenz [1984, 1990] derived the chaotic behavior from an interaction between unstable transient waves and a thermally

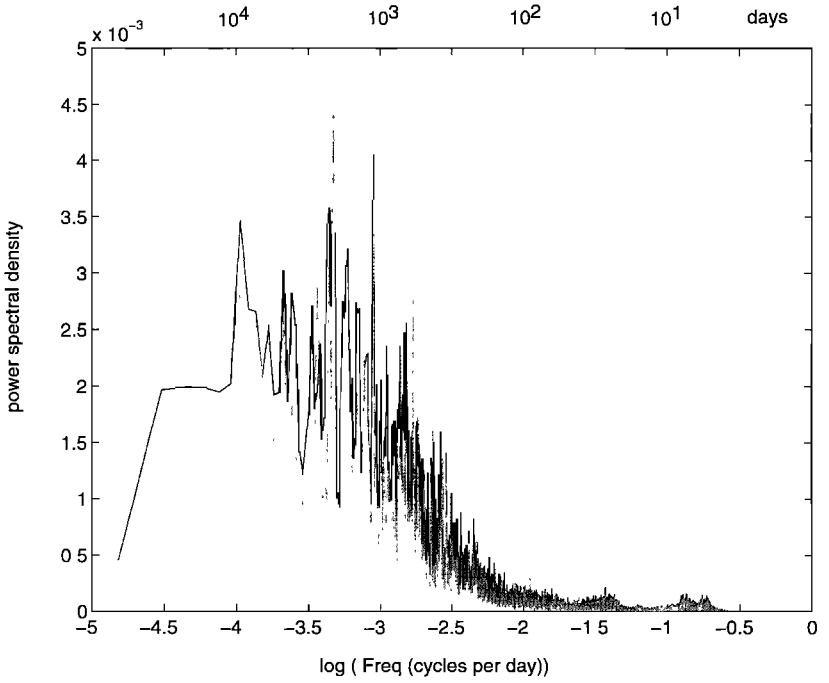

Figure 12. Run 2: Power spectrum P_α as a function of the logarithm of frequency computed from 400,000 days of α for $m = 2$, $n = 5$, $N = 3$, $h = 2500$ m, and $Ro_T = 0.07$ (70°C) with seasonal forcing. The power spectrum is shown by the bold black line, and the half width of the 95% confidence interval is shown by the thin gray line.

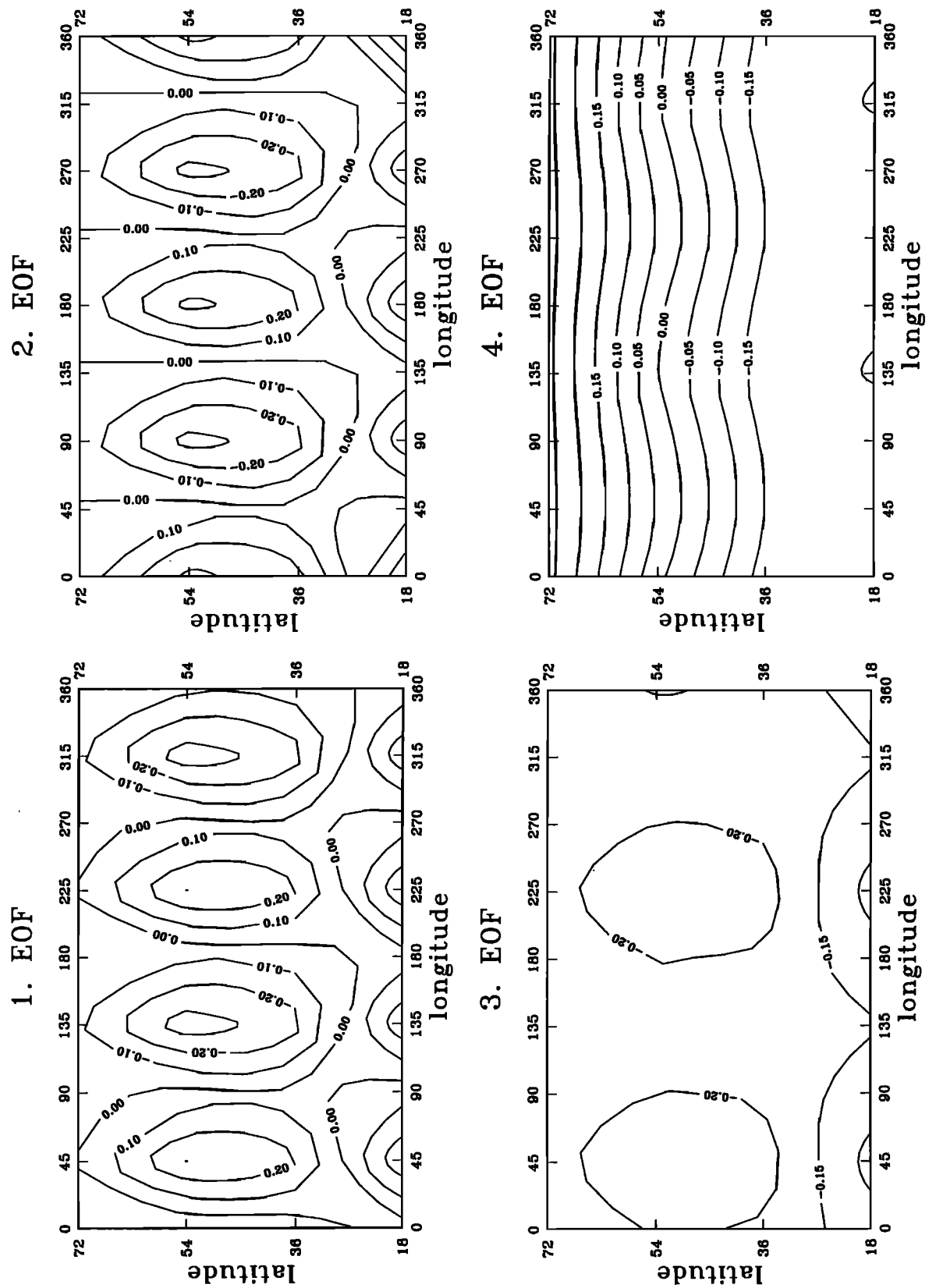

Figure 13. Run 2: Structure of EOFs 1, 2, 3, and 4. The EOFs are normalized by unity.

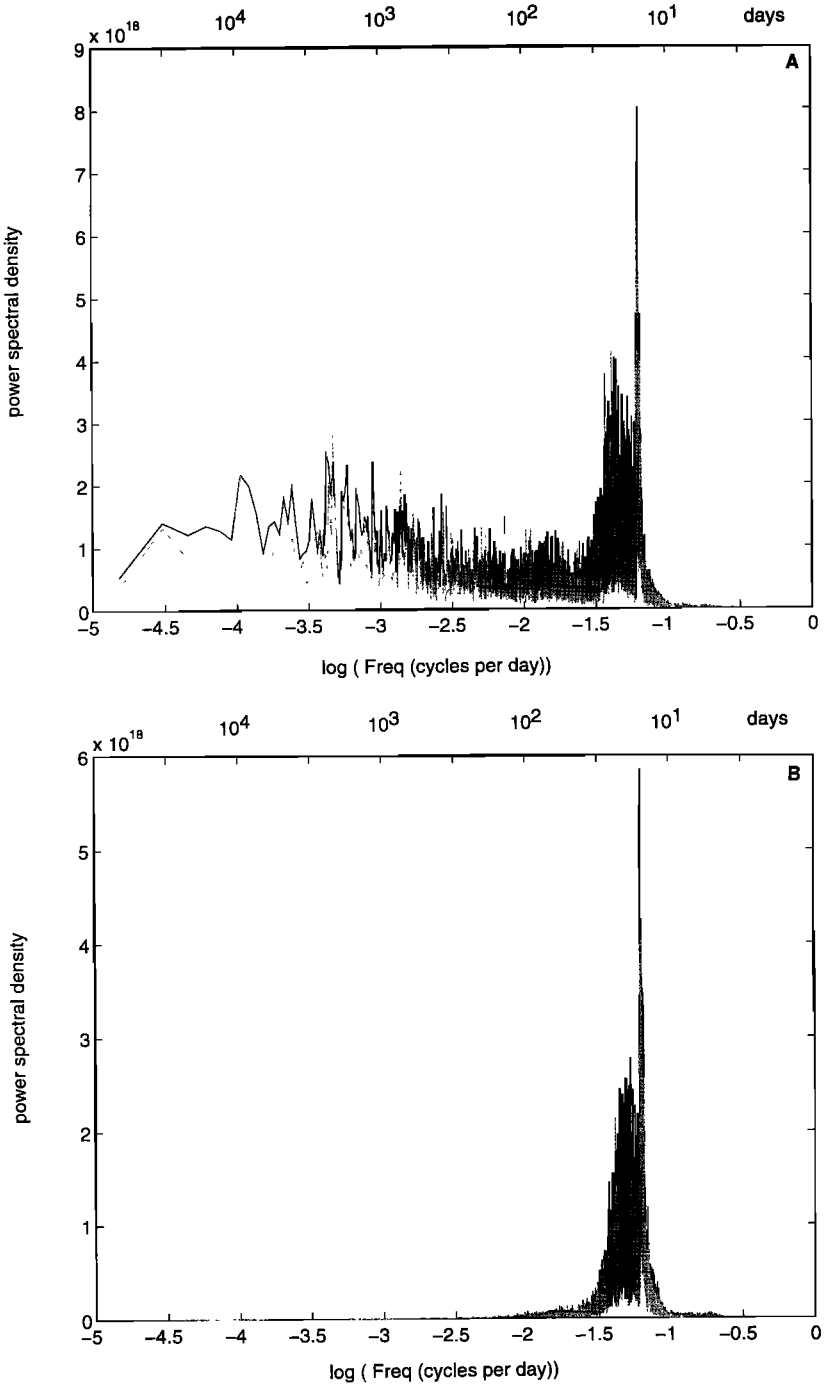

Figure 14. Run 2: Power spectrum of (a) PC 1, (b) PC 2, (c) PC 3, and (d) PC 4. Notation as in Figure 12.

forced steady wave. *James and James* [1992] included neither orographic nor nonzonal thermal forcing. Contrary to these authors the chaotic behavior in our model is due to the interaction between the orographically forced standing waves with the zonal mean state. We cannot exclude that the transients inherent in our model also play an important role for long-term climate variability. The inclusion of the seasonal cycle leads to structural changes of the EOF 3 and EOF 4 and in the high-frequency part of the power spectra of PC 3 and PC 4, indicating the important role of transients in the long-term variability.

We have shown that long-term climatic variability on time-scales of decades can originate from energetic imbalances in the atmosphere from year to year due to nonlinear dynamics connected with wave mean flow interactions under the control of a seasonal course. A similar result was obtained by *James and James* [1992] in a spectral primitive equation model with moderate resolution of dynamical processes and by *Pielke and Zeng* [1994] in a low-resolution model. Our model is very simple, and it assumes only a thermal forcing on the zonal component and an orographic forcing in the long wave. We have got a chaotic solution behavior using realistic parameter

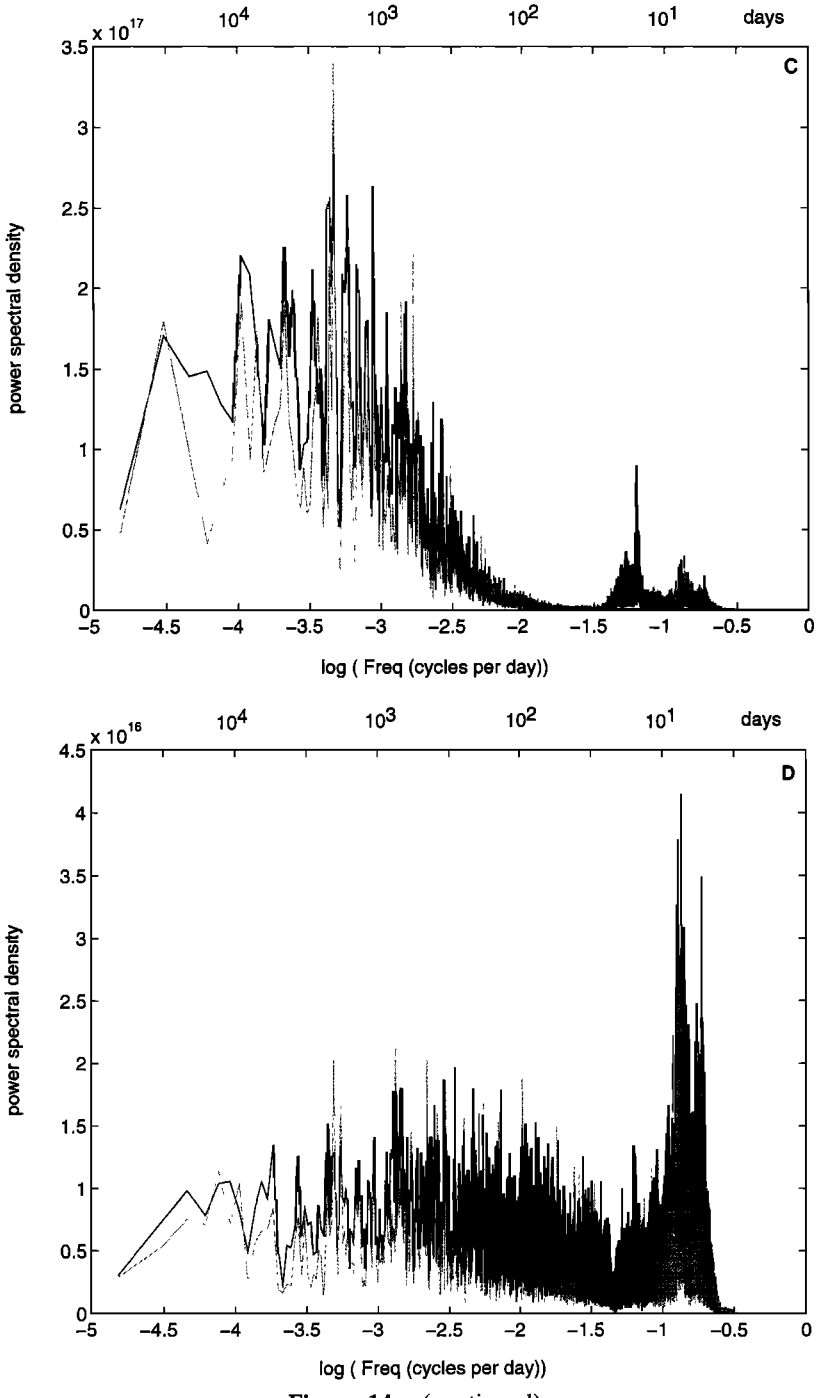

Figure 14. (continued)

Table 1. Total Variance σ_α^2 for Different Intervals of Periods Without and With Seasonal Cycle of Nondimensional Amplitude E

Period	σ_α^2, %	
	Run 1 (E = 0)	Run 2 (E = 2/7)
2 days to 6 days	13.0	2.6
6 days to 1.1 year	53.4	92.7
1.1 year to 11 years	27.2	4.1
11 years to 1100 years	6.4	0.6

values and obtained a natural variability in decadal time scales. It is possible to improve this simple model by including baroclinic unstable waves and nonlinear interaction between long and synoptic waves as was done by *Dethloff and Schmitz* [1992]. Currently, our model is too simple to be used directly for quantitative studies of long-term climatic changes. Nevertheless, it confirms the idea that seasonal forcing together with nonlinear dynamical processes can generate long-term variability between 10^0 and 10^2 years in the atmosphere without additional external forcing.

Appendix A

The spectral form of equations (11)–(12) consists of the following 8 ordinary nonlinear differential equations (overdots denote the derivative d/dt):

$$\tfrac{2}{3}[2 + \Lambda^2(1 - \varepsilon)]\dot{\alpha} + \tfrac{1}{2}m\Lambda^2(AB - KL) + \tfrac{1}{2}m\Lambda^2(1 - \varepsilon)\mathrm{H}_0K - \tfrac{1}{2}m\Lambda^2\mathrm{H}_0B + \tfrac{4}{3}C(\alpha - \beta) - \tfrac{2}{3}\Lambda^2Q(\beta^* - \beta) = 0, \quad \text{(A1)}$$

$$[N(N + 1) + \Lambda^2(1 - \varepsilon)]\dot{F} - \tfrac{1}{2}mq\Lambda^2(AB - KL) - \tfrac{1}{2}mq\Lambda^2(1 - \varepsilon)\mathrm{H}_0K + \tfrac{1}{2}mq\Lambda^2\mathrm{H}_0B + CN(N + 1)(F - G) + \Lambda^2QG = 0, \quad \text{(A2)}$$

$$[n(n + 1) + \Lambda^2(1 - \varepsilon)]\dot{A} - \alpha m\Lambda^2B + [2(1 + k\alpha) + \beta\Lambda^2 - k\alpha n(n + 1)]mK - kmq[N(N + 1) - n(n + 1)]KF + mq\Lambda^2(BF - KG) + Cn(n + 1)(A - L) + \Lambda^2QL = 0, \quad \text{(A3)}$$

$$[n(n + 1) + \Lambda^2(1 - \varepsilon)]\dot{K} + \alpha m\Lambda^2L - [2(1 + k\alpha) + \beta\Lambda^2 - k\alpha n(n + 1)]mA + kmq[N(N + 1) - n(n + 1)]AF - mq\Lambda^2(FL - AG) - \alpha m\Lambda^2(1 - \varepsilon)\mathrm{H}_0 + mq\Lambda^2(1 - \varepsilon)\mathrm{H}_0F - mq\Lambda^2\mathrm{H}_0G + \beta m\Lambda^2\mathrm{H}_0 + Cn(n + 1)(K - B) + \Lambda^2QB = 0, \quad \text{(A4)}$$

$$\tfrac{2}{3}[2 + \Lambda^2(1 - \varepsilon)]\dot{\beta} + \tfrac{1}{2}m(2 + \Lambda^2)(AB - KL) - \varepsilon m\mathrm{H}_0K - \tfrac{1}{2}\varepsilon m\Lambda^2\mathrm{H}_0B - \tfrac{4}{3}\varepsilon C(\beta - \alpha) - \tfrac{2}{3}(2 + \Lambda^2)Q(\beta^* - \beta) = 0, \quad \text{(A5)}$$

$$[N(N + 1) + \Lambda^2(1 - \varepsilon)]\dot{G} - \tfrac{1}{2}mq[N(N + 1) + \Lambda^2] \cdot (AB - KL) - \tfrac{1}{2}\varepsilon mqN(N + 1)\mathrm{H}_0K - \tfrac{1}{2}\varepsilon mq\Lambda^2\mathrm{H}_0B - \varepsilon CN(N + 1)(G - F) + [N(N + 1) + \Lambda^2]QG = 0, \quad \text{(A6)}$$

$$[n(n + 1) + \Lambda^2(1 - \varepsilon)]\dot{B} + \alpha m[n(n + 1) + \Lambda^2]L - m \cdot [\beta n(n + 1) + \beta\Lambda^2 + 2\varepsilon(1 + k\alpha) - \varepsilon k\alpha n(n + 1)]A - mq[n(n + 1) + \Lambda^2](FL - AG) - \varepsilon kmq[N(N + 1) - n(n + 1)]AF + \varepsilon\alpha mn(n + 1)\mathrm{H}_0 + \varepsilon\beta m\Lambda^2\mathrm{H}_0 - \varepsilon mqn(n + 1)\mathrm{H}_0F - \varepsilon mq\Lambda^2\mathrm{H}_0G - \varepsilon Cn(n + 1)(B - K) + Q[n(n + 1) + \Lambda^2]B = 0, \quad \text{(A7)}$$

$$[n(n + 1) + \Lambda^2(1 - \varepsilon)]\dot{L} - \alpha m[n(n + 1) + \Lambda^2] \cdot B + m[\beta n(n + 1) + \beta\Lambda^2 + 2\varepsilon(1 + k\alpha) - \varepsilon k\alpha n(n + 1)]K + mq[n(n + 1) + \Lambda^2](BF - KG) + \varepsilon kmq[N(N + 1) - n(n + 1)]KF - \varepsilon Cn(n + 1)(L - A) + Q[n(n + 1) + \Lambda^2]L = 0. \quad \text{(A8)}$$

Here,

$$q = \int_{-1}^{1} (P_n^m)^2(dP_N^0/d\mu)d\mu$$

is the so-called interaction coefficient. When, for example, $m = 2$, $n = 5$, and $N = 5$, then $q = (20/13)\sqrt{11/2} \cong 3.608$, and in the case of $m = 2$, $n = 5$, and $N = 3$ one has $q \cong 3.310$.

Appendix B

If variables α and β are the prescribed constants, then equations (A1)–(A8) reduce to a system of six ordinary differential equations. Below, these are written in a symbolic form using a new timescale $t_1 = [n(n + 1) + \Lambda^2(1 - \varepsilon)]^{-1}t$ and for a special case of $\alpha = \beta = \text{const}$, $k = 1$, $n = N$, and $\mathrm{H}_0 = 0$:

$$F' + \tfrac{1}{2}\Pi(KL - AB) = 0, \quad \text{(B1a)}$$

$$A' + \mathrm{M}K - \mathrm{N}B + \Pi(BF - KG) = 0, \quad \text{(B1b)}$$

$$K' - \mathrm{M}A + \mathrm{N}L - \Pi(LF - AG) = 0, \quad \text{(B1c)}$$

$$G' + \tfrac{1}{2}\mathrm{X}(KL - AB) = 0, \quad \text{(B1d)}$$

$$B' - \mathrm{Y}A + \mathrm{Z}L - \mathrm{X}(LF - AG) = 0, \quad \text{(B1e)}$$

$$L' + \mathrm{Y}K - \mathrm{Z}B + \mathrm{X}(BF - KG) = 0. \quad \text{(B1f)}$$

Here

$$\Pi = mq\Lambda^2;\ \mathrm{X} = mq[n(n + 1) + \Lambda^2],$$

$$\mathrm{M} = m[2(1 + \alpha) + \alpha\Lambda^2 - \alpha n(n + 1)],\ \mathrm{N} = \alpha m\Lambda^2,$$

$$\mathrm{Y} = m[2\varepsilon(1 + \alpha) + \alpha\Lambda^2 + \alpha n(n + 1)(1 - \varepsilon)],$$

$$\mathrm{Z} = m\alpha[n(n + 1) + \Lambda^2],$$

and the prime denotes a derivative d/dt_1.

Equations (B1) have the linearly independent integrals of motion, written in the following convenient form:

$$\Pi G - \mathrm{X}F = C_1,$$

$$\tfrac{1}{2}(A^2 + K^2) - 2\mathrm{N}\Pi^{-1}F + F^2 = C_2,$$

$$\tfrac{1}{2}(B^2 + L^2) - 2\mathrm{Y}\mathrm{X}^{-1}G + G^2 = C_3,$$

$$AL + BK - 2\mathrm{X}^{-1}(\mathrm{M} + \mathrm{Z} + C_1)G + 2\Pi\mathrm{X}^{-1}G^2 = C_4.$$

Their linear combinations reflect the mass, energy, and entropy conservation laws, and also the integral form of Ertel's potential vorticity conservation law.

With the help of these integrals, equations (B1) reduce to the single equation

$$G'' + A_1G^2 + A_2G + A_3 = 0, \quad \text{(B2)}$$

where

$$A_1 = 3\mathrm{X}^{-1}[\mathrm{X}^2\mathrm{N} + \Pi^2\mathrm{Y} - (\mathrm{M} + \mathrm{Z})\mathrm{X}\Pi],$$

$$A_2 = (\mathrm{M} + \mathrm{Z})^2 - 4\mathrm{Y}\mathrm{N} + \mathrm{X}^2C_2 + \Pi^2C_3 - \mathrm{X}\Pi C_4 + 2C_1(\mathrm{M} + \mathrm{Z}) - C_1(\mathrm{N}\mathrm{X}\Pi^{-1} + 2\mathrm{Y}\Pi\mathrm{X}^{-1}),$$

$$A_3 = \tfrac{1}{2}X(M + Z)C_4 - YXC_2 - NXC_3 + \tfrac{1}{2}XC_1C_4 + YX^{-1}C_1^2 - \Pi C_1C_3 + 2YN\Pi^{-1}C_1.$$

Given initial conditions, equation (B2) has an exact solution in terms of elliptic functions. Multiplying (B2) by G' and integrating in time, we obtain

$$\tfrac{1}{2}(G')^2 + \tfrac{1}{3}A_1G^3 + \tfrac{1}{2}A_2G^2 + A_3G + A_4 = 0, \quad \text{(B3)}$$

where a constant A_4 is determined by the initial conditions. In terms of variables

$$\wp = -G - \tfrac{1}{2}(A_2/A_1), \qquad U = t_1(A_1/6)^{1/2}, \qquad A_1 > 0$$

equation (B3) takes the normal Weierstrass' form [see *Abramowitz and Stegun*, 1964, and references therein]

$$(d\wp/dU)^2 = 4\wp^3 - g_2\wp - g_3.$$

Here

$$g_2 = 3(A_2/A_1)^2 - 12(A_3/A_1),$$

$$g_3 = \tfrac{1}{2}(A_2/A_1)^3 - 6(A_2A_3/A_1^2) + 12(A_4/A_1).$$

In particular, it is possible to express the period of nonlinear oscillations resulting in the model in terms of a complete elliptic integral of the first kind. This property has been used for testing the numerical procedure outlined in the main part of the paper.

Acknowledgments. We gratefully acknowledge the help of Eduard Claudius and Uwe Eggert (Alfred Wegener Institute (AWI), Potsdam) in solving numerical problems. We further thank Dirk Olbers and Christoph Völker (AWI Bremerhaven), Annette Rinke and Justus Notholt (AWI Potsdam), and Jürgen Kurths (University of Potsdam) for helpful discussions. The computations were carried out during two visits of M.V.K. as guest scientist at the AWI Potsdam. M.V.K. and I.A.P. are grateful for the support by the Russian Foundation for Fundamental Investigations (RFFI) under project grant 94-05-16356. The authors appreciate the helpful suggestions by the two anonymous reviewers, which have lead to great improvements. Alfred Wegener Institute for Polar and Marine Research contribution 777.

References

Abramowitz, M., and I. A. Stegun (Eds.), *Handbook of Mathematical Functions, Graphs and Mathematical Tables, Appl. Math. Ser.*, vol. 55, U.S. Govt. Print. Off., Washington, D. C., 1964.

Alishayev, D. M., Dynamics of the two-dimensional baroclinic atmosphere, *Izv. Acad. Sci. USSR Atmos. Oceanic Phys.*, Engl. Transl., *16*, 63–67, 1980.

Alishayev, D. M., Large-scale dynamics of a two-dimensional baroclinic diabatic atmosphere, *Izv. Acad. Sci. USSR Atmos. Oceanic Physics*, Engl. Transl., *17*, 93–97, 1981.

Berger, A., M.-F. Loutre, and C. Tricot, Insolation and Earth's orbital periods, *J. Geophys. Res.*, *98*, 12,839–12,847, 1993.

Birchfield, G. E., and M. Ghil, Climate evolution in the Pliocene and Pleistocene from marine sediment records and simulations: Internal variability versus orbital forcing, *J. Geophys. Res.*, *98*, 10,385–10,399, 1993.

Branstator, G., and I. Held, Westward propagating normal modes in the presence of stationary background waves, *J. Atmos. Sci.*, *52*, 247–262, 1995.

Charney, J. G., On a physical basis for numerical prediction of large-scale motions in the atmosphere, *J. Meteorol.*, *6*, 371–385, 1949.

Dethloff, K., and G. Schmitz, Persistent circulation states and low-frequency variability in a nonlinear, baroclinic low-order model, *Meteorol. Z.*, *1*, 141–154, 1992.

Dutton, J. A., The global thermodynamics of atmospheric motion, *Tellus*, *25*, 89–111, 1973.

Egger, J., Point vortices in a low order model of barotropic flow on the sphere, *Q. J. R. Meteorol. Soc.*, *118*, 533–552, 1992.

Galin, M. B., and C. E. Kirichkov, Stability of atmospheric zonal circulation in a model including orography and the blocking problem, (in Russian), *Izv. Akad. Nauk SSSR Fiz. Atmos. Okeana*, *21*, 563–572, 1985. (English translation, *Izv. Acad. Sci. USSR Atmos. Oceanic Phys.*, Engl. Transl., *21*, 433–439, 1985.)

Ghil, M., Nonlinear approaches to low-frequency atmospheric variability, in *Dynamics of Low-Frequency Phenomena in the Atmosphere*, edited by G. Branstator et al., pp. 603–714, Boulder, Colo., 1988.

Haines, K., Low-frequency variability in atmospheric middle latitudes, *Surv. Geophys.*, *15*, 1–63, 1994.

James, I. N., and P. M. James, Spatial structure of ultra-low-frequency variability of the flow in a simple atmospheric circulation model, *Q. J. R. Meteorol. Soc.*, *118*, 1211–1233, 1992.

Kaplan, J. L., and J. A. Yorke, Chaotic behavior of multidimensional difference equations, in *Functional Differential Equations and Approximation of Fixed Points*, edited by H. O. Peitgen and H. O. Walther, pp. 228–237, Springer-Verlag, New York, 1979.

Kurgansky, M. V., On the integral energy characteristics of the atmosphere (in Russian), *Izv. Akad Izvestiya. Nauk. SSSR Fiz. Atmos. Okeana*, *17*, 923–933, 1981. (English translation, *Izv. Acad. Sci. USSR Atmos. Oceanic Phys.*, Engl. Transl., *17*, 686–692, 1981.)

Lorenz, E. N., Irregularity: A fundamental property of the atmosphere, *Tellus, Ser. A*, *36*, 98–110, 1984.

Lorenz, E. N., Can chaos and intransitivity lead to interannual variability?, *Tellus, Ser. A*, *42*, 378–389, 1990.

Marquet, P., On the concept of energy and available enthalpy: Application to atmospheric energetics, *Q. J. R. Meteorol. Soc.*, *117*, 449–475, 1991.

Mayewski, P. A., L. D. Meeker, M. C. Morrison, M. S. Twickler, S. I. Whitlow, K. K. Ferland, D. A. Meese, M. R. Legrand, and J. P. Steffenson, Greenland ice core "signal" characteristics: An expanded view of climate change, *J. Geophys. Res.*, *98*, 12,839–12,847, 1993.

Pielke, R. A., and H. Zeng, Long-term variability of climate, *J. Atmos. Sci.*, *51*, 155–159, 1994.

Pearce, R. P., On the concept of available potential energy, *Q. J. R. Meteorol. Soc.*, *104*, 737–755, 1978.

Shimada, J., and T. Nagashima, A numerical approach to ergodic problem of dissipative dynamic systems, *Prog. Theor. Phys.*, *61*, 1605–1616, 1979.

Tennekes, H., The general circulation of two-dimensional turbulent flow on a beta-plane, *J. Atmos. Sci.*, *34*, 702–712, 1977.

Wallace, J. M., The climatological mean stationary waves: observational evidence, in *Large-Scale Processes in the Atmosphere*, edited by B. J. Hoskins and R. P. Pearce, pp. 27–54, Academic, San Diego, Calif., 1983.

F. M. Chmielewski, Meteorological Institute, Humboldt Universität, Müggelseedamm 256, D-12587 Berlin, Federal Republic of Germany.

K. Dethloff and H. Gernandt, Alfred-Wegener-Institut fur Polar- und Meeresforschung, Telegraphenberg A.43, D-14473 Potsdam, Federal Republic of Germany. (e-mail: dethloff@awi-potsdam.de)

W. Jansen, Department of Nonlinear Dynamics, Universität Potsdam, Am Neuen Palais 10, D-14415 Potsdam, Federal Republic of Germany.

M. V. Kurgansky and I. A. Pisnichenko, Institute of Atmospheric Physics, Russian Academy of Sciences, Pyzhevsky 3, 109017 Moscow, Russia.

(Received July 20, 1994; revised April 17, 1995; accepted August 29, 1995.)